An acquisition system that extracts the earth response from seismic data

Gregg Parkes[1] and Stian Hegna[1*] focus on new developments in source technology for marine seismic acquisition aimed at removing all the acquisition-related effects.

The objective of the seismic method has always been to map the response of the earth. However, acquisition-imposed effects are incorporated in the seismic data limiting our ability to achieve this. These acquisition-related effects are the two sea surface reflections (ghosts), and the response of the source and the receiver systems. In 2007 dual sensor streamers were introduced to the marine seismic exploration industry. This technology allowed the receiver-side sea surface reflection to be removed from seismic data (e.g., Carlson et al., 2007). The response of the receiver system is broadband and well known, so this term can also be handled. This leaves the source response and the source ghost. This paper will show methodologies to treat both these terms to complete the system and remove all the acquisition-related effects from seismic data to reveal the response of the earth.

At this point it is worthwhile reviewing the properties of source and receiver ghosts to understand the benefits of removing them. The left hand side of Figure 1 schematically shows how the wavefield propagating into the earth from the source is made up of a direct component and a sea surface reflection component. In an exactly analogous way on the receiver side, the recorded wave field is made up of the arrival directly scattered from the earth combined with a second sea surface reflection component. The reflection coefficient at the sea surface is very close to -1, resulting in a close to perfect reflection, as well as a phase change. The individual ghost functions on the source and receiver side are shown in the centre of Figure 1. These dipole functions create notches in the spectrum, at frequencies that depend on the respective depths of the source and receiver. The right hand side of Figure 1 shows how the source and receiver ghost functions combine together to form an elongated wavelet. The corresponding spectrum contains two sets of notches.

Figure 2 shows essentially the reverse of Figure 1. It illustrates the effect when first the receiver ghost is removed and then the source ghost is removed from the combined source and receiver ghosts. In the first step the wavelet becomes shorter in time, but in the second step it reduces to a single spike, with a notch-free, flat spectrum.

A primary motivation for developing a ghost-free acquisition system was exactly the effect shown in Figure 2. That is, reducing the extended combined ghost function of source and receiver to a single spike. The resultant effect on the resolution of the seismic data is extremely significant and this will be shown in a later section. However, the scale of the effect can be illustrated using the photograph in Figure 3. The top photograph contains two ghosts which have been added with

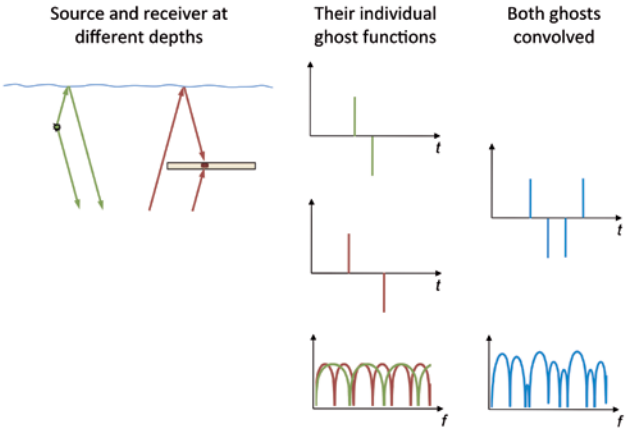

Figure 1 *Illustration of the sea surface reflections that cause ghosts on both the source and receiver side. The individual ghost functions and their spectra are shown in the centre along with the combined function and amplitude spectrum on the right.*

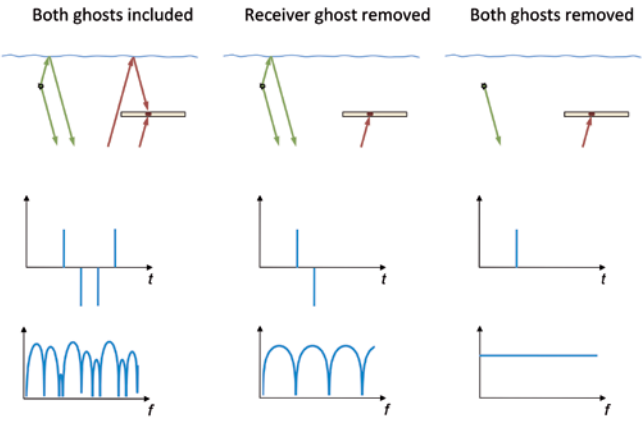

Figure 2 *Illustration of the effect of removing the receiver ghost and then source ghost, in turn. In the first step the wavelet becomes shorter in time, but in the second step it becomes a single spike. Similarly, in the spectrum, the two sets of ghost notches are removed to end up with a flat spectrum.*

[1] *Petroleum Geo-Services.*
[*] *Corresponding author, E-mail: stian.hena@pgs.com*

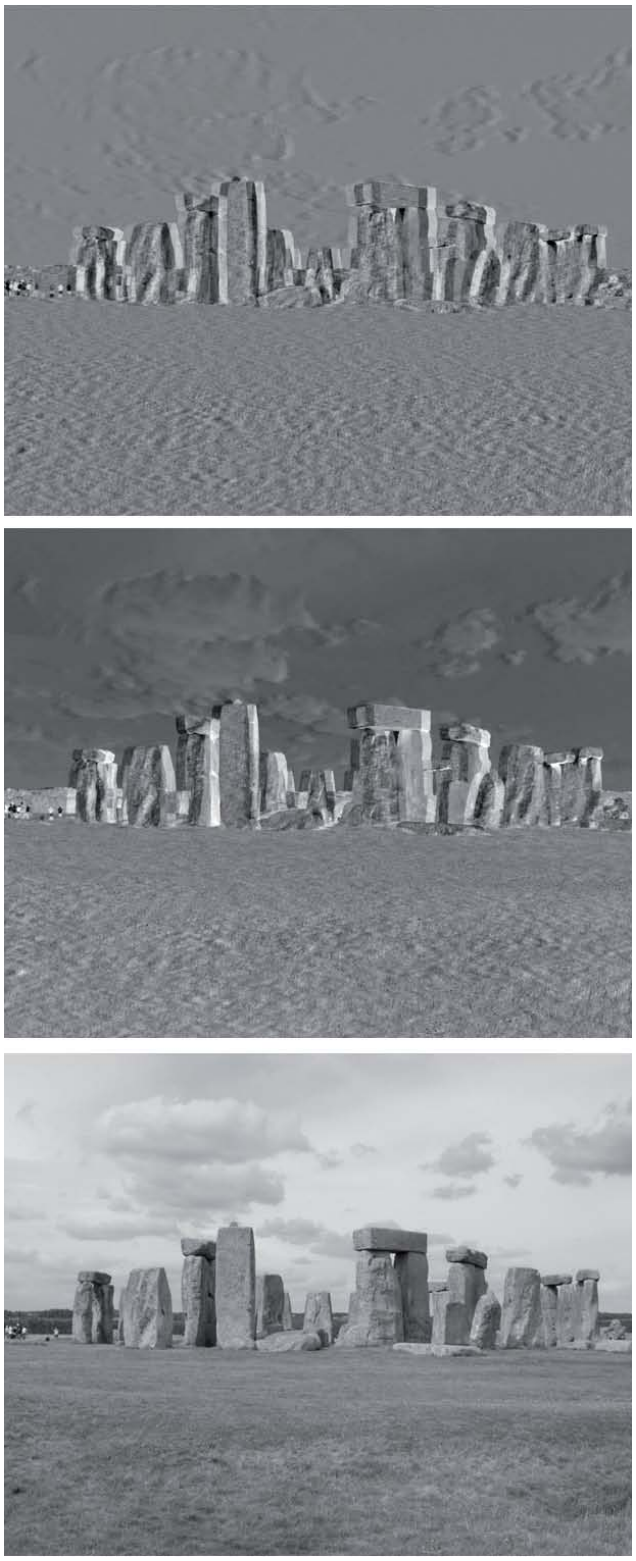

Figure 3 *Photograph of Stonehenge in Wiltshire, England. The top photo has had 2 ghosts added, in a way that is completely analogous to the effects of sea surface ghosts. The central photo has a single ghost and the bottom photo no ghosts. This illustrates the very large effect that removing both ghosts has on the resolution.*

exactly the same polarity reversal as the two sea surface ghosts. The vertical structures clearly show two distinct bands (one black and one white) to their right hand side. The centre photograph contains only a single ghost (white band on the right). This picture is clearer but is still significantly out of focus because of the single ghost. The bottom photograph is ghost-free, equivalent to the single spike of Figure 2. The resolution in this case is only limited by the intrinsic bandwidth (pixel resolution) of the photograph. Removing one ghost is clearly a significant improvement, but the combination of removing both ghosts brings the picture into complete focus. The effect in seismic data is completely analogous, which will be demonstrated in a later section.

As discussed before, technology for removing the receiver-side ghost is already well known, so this paper will concentrate on the source response and the source ghost. In particular, a technology on the source side has been developed to provide the full ghost-free solution discussed above.

Removing the source ghost

The new source design that allows the source ghost to be removed is distributed in both time and depth. The source array is divided into sub-sources, and each sub-source is deployed at a specific depth and fired with specific firing time delays. The depths of the sub-sources are chosen such that the ghost functions are complementary, avoiding deep notches in the spectrum. Figure 4 schematically illustrates complementary ghost functions from sources deployed at two different depths.

The firing time delays of the sub-sources within the full array would generally be less than 1 second. This means that the geology illuminated by each sub-source is essentially identical, and the receivers are in the same locations when the sub-sources fire. In addition, this source can be fired with the same shot efficiency and density as a conventional source. These features of the geometry are a key in the processing of the seismic data.

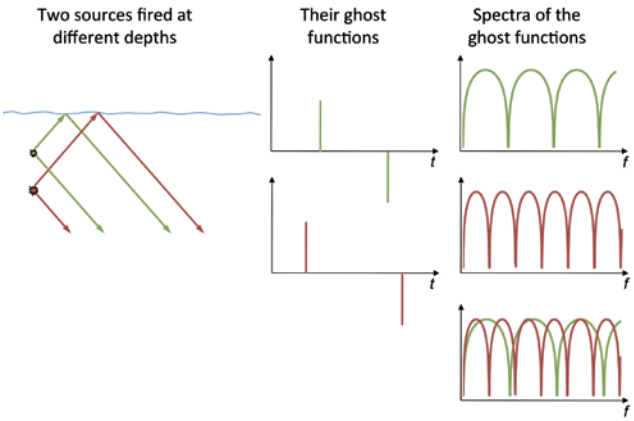

Figure 4 *Ghosts from sources deployed at different depths with corresponding spectra, to illustrate how they complement each other.*

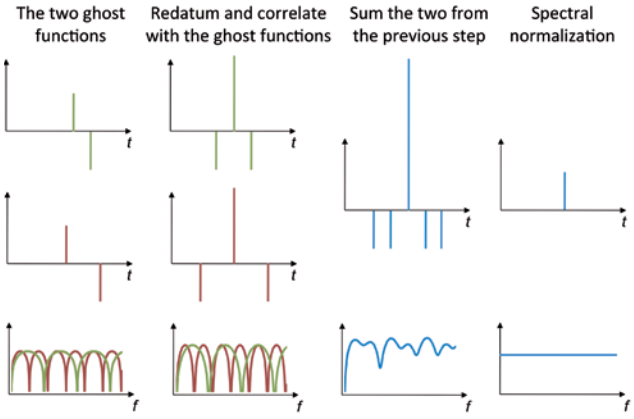

Figure 5 *Illustration of the ghost removal process starting off with two ghost functions. The ghost functions are then correlated with themselves resulting in the auto-correlation of the ghost functions, followed by a summation of the two auto-correlations, and finally a spectral normalization.*

The processing of the seismic data includes separating the wavefields emitted by the sub-sources, followed by re-combining these wavefields in such a way that the source ghost is removed. The separation of the wavefields emitted by the sub-sources utilizes the known firing time delays to perform a robust separation. The fact that the sub-sources are firing in nearly the same locations may also be beneficial in this process. In addition, the subsequent source ghost removal step involving re-combining those wavefields improves the accuracy of the end results, since any residual energy is greatly suppressed in this step.

The method used for removing the receiver ghost is already well-known. However the methodology on the source side is somewhat different. With sub-sources deployed at different depths, the source ghost can be removed through a weighted summation of the wavefields emitted by the sub-sources. A method for doing this is described in Posthumus (1993). The process of removing the ghosts is schematically illustrated in Figure 5. This figure shows the two ghost functions input to the ghost removal process in step 1. Step 2 shows the results after aligning the peaks to compensate for the differences in depths and correlating with the ghost functions. Step 3 shows the results after summing the auto-correlation of the ghost functions from step 2, and step 4 shows the results after the final spectral normalization. The source ghost removal process is done in an angle dependent fashion.

The source ghost removal process with sub-sources deployed at different depths is very robust, provided that the depths are chosen such that the ghost functions are complementary. Figure 6 illustrates the spectral errors introduced if there is a +/-0.5 m depth error in the assumptions when removing the source ghost using the method illustrated in Figure 5, and when de-ghosting data from a conventional source. The depth of the conventional source was 8 m, and the depths of the sub-sources in the new source design were 5 m and 8 m. The depth errors were introduced into the 8 m sub-source.

The new methodology has many advantages, not least of which is the robustness of the ghost removal, as described above. Of course, as a direct result of this there are no source-related ghost notches in the spectrum of the resultant seismic data. This means that the source can be deployed at a wider range of depths, within practical limits. In particular, sub-sources can be deployed at depths that give a high signal to noise ratio (S/N) towards lower frequencies while maintaining a high S/N at high frequencies, providing very broadband seismic data.

The physical behaviour of airguns has implications on the low frequency signal levels when sources are deployed at larger depths. Figure 7 illustrates far-field signatures including the source ghosts modelled at depths of 5, 10, and 15 m. When air-guns are deployed at greater depths, the bubble periods become shorter resulting in higher fundamental frequencies. This effect largely counteracts the reduction in attenuation caused by the change in the ghost function at the very low frequency end. This effect is discussed in detail in Hegna and Parkes (2011). Figure 7 shows that there is very little change in the output signal levels below ~7 Hz when the source depth is increased from 5 m to 10 m and further

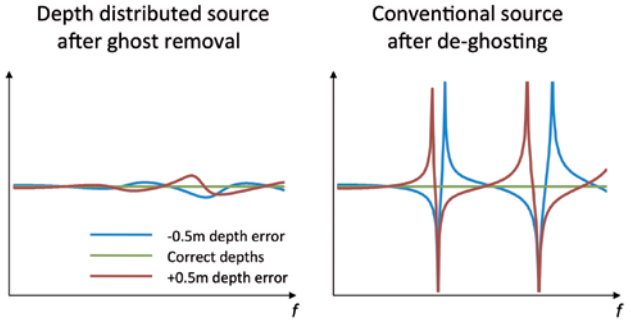

Figure 6 *Robustness to depth errors when removing the ghost from a depth distributed source compared to de-ghosting data from a conventional source. The frequency axis ranges from 0 to 250 Hz, whereas the vertical amplitude axis ranges from -30 to+30 dB.*

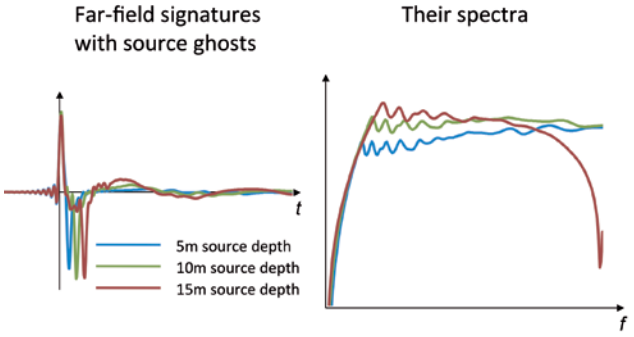

Figure 7 *Far-field signatures including the source ghosts and corresponding spectra modelled at 5 m, 10 m and 15 m source depths. The time axis ranges from -50 to 250 ms. In the plot of the spectra, the frequency axis ranges from 0 to 50 Hz, and the amplitude axis covers a 60 dB range.*

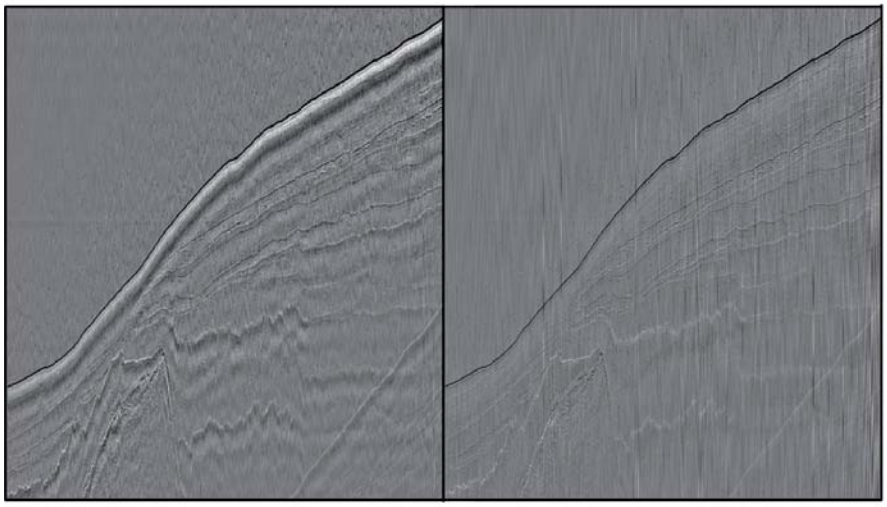

Figure 8 *Single near trace data after source and receiver de-ghosting. The plot on the left still contains the ghost-free source response, whereas on the right this response has been deconvolved.*

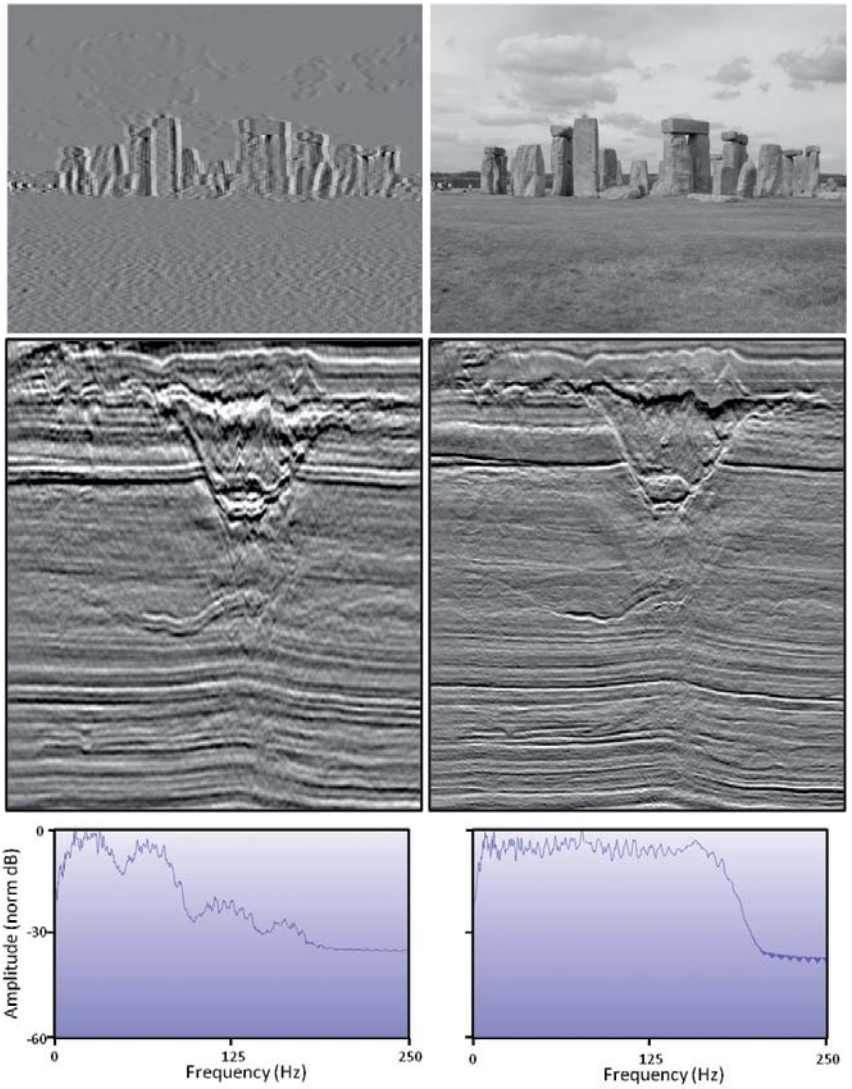

Figure 9 *The top two photographs are of Stonehenge, the left of which contains two ghosts and the right none. The centre plots show conventional seismic data on the left and data obtained with the dual sensor streamer and time and depth blended source on the right. This second dataset has had all the acquisition related effects removed, as described in the text. The bottom plots are the spectra of the seismic data.*

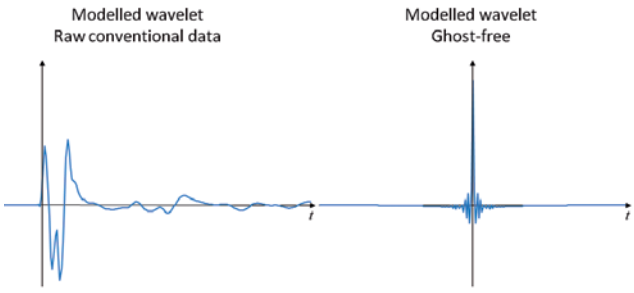

Figure 10 *The modelled seismic wavelet in raw conventional data (left) and in the processed ghost-free data (right). The time axis ranges from -50 to +350 ms to the left and from -200 to +200 ms on the right. A large and beneficial change in phase characteristics takes place in the wavelet transformation.*

to 15 m. However, between ~7 and ~30 Hz, the increase in signal level is up to 12 dB (maximum increase at ~10 Hz), corresponding to a factor of four when the source depth is increased from 5 to 15 m. This makes the system ideal for maximizing the illumination of deep targets. Furthermore, with a time and depth blended source this is achieved with minimal compromises to the S/N at high frequencies, due to the complementary ghost functions from the sub-sources towed at different depths. In combination with the dual sensor streamer technology, the result is a ghost-free broadband solution with a high S/N over a very large frequency band. In addition, this acquisition-based solution enables the removal of both the source and the receiver ghosts at an early stage in the pre-processing sequence, and produces high quality pre-stack as well as post- stack data. It has been demonstrated that the removal of the receiver-side ghost is beneficial for processing steps such as multiple suppression and velocity analysis (e.g., Van Borselen et al., 2011; Long et al., 2008). It follows that the removal of the source ghost in addition will be similarly beneficial.

Removing the source response

The previous section has concentrated on the ghosts. However, the intrinsic source response, which is now ghost-free, remains in the data. The form of this response is well-known and results from the oscillatory nature of airgun bubbles. In fact, the bubble train in the ghost-free response is more visible than in the ghosted response because the ghosts significantly attenuate the lower frequencies. In addition, the complexity of the bubble train is reduced with a ghost-free response. The prior removal of the ghost creates an important advantage at this stage. That is, the remaining response

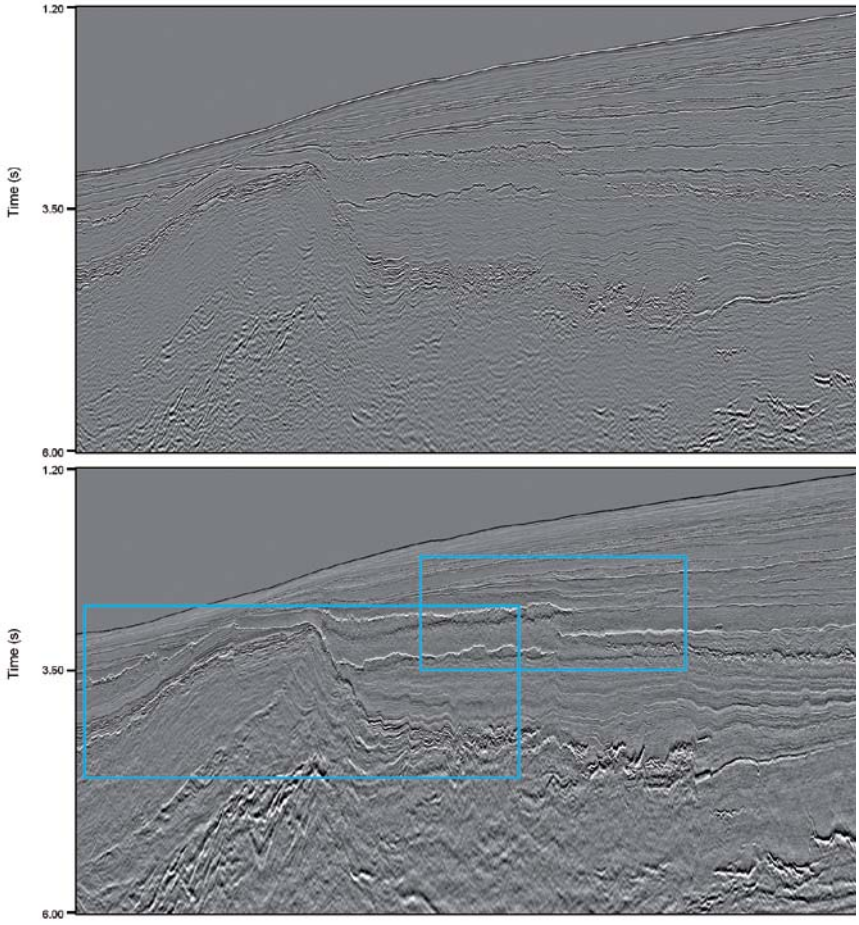

Figure 11 *Data from the More margin region of the Norwegian sea. The top section represents conventional seismic data, whereas the bottom section was shot separately with the system that allows all the acquisition effects to be removed from the data.*

(or signature) does not have notches in its spectrum, so a very robust deconvolution operator can be designed. This operator must be designed from responses that include the effects of the differences in bubble periods between the different depths of the sub-sources. The filter applies a large phase correction to compress the bubble train onto the primary, as well as normalizing for the amplitude variation with frequency.

The effect of de-convolving the source response is illustrated in Figure 8. The left hand plot shows a single near-trace, which has undergone both source and receiver ghost removals using a 1D approximation. The source response, which looks like a low frequency reverberation, can be clearly seen under the water bottom reflection. The right hand plot shows the same data after the source response has been deconvolved. The reverberation has now gone and the events in the data look much sharper due to the broadband nature of these data. The source response in this example was calculated from near-field measurements made on the source array, however there are several alternative possibilities.

Revealing the earth response

As discussed above, seismic data are constrained by acquisition-imposed effects and there has never been a good solution for eliminating all these constraints. With the dual sensor streamer and time and depth blended source, the source and receiver ghosts can be eliminated in a robust fashion. The response of the source system, after the source ghost has been removed, can be deconvolved in a robust deterministic way. After going through these steps, only the response of the receiver system is left. This is typically a broadband response covering the entire spectrum of interest. Therefore, it is not necessary to correct for it. However, since it is a very well known response, it can be re-shaped for example to its zero phase equivalent.

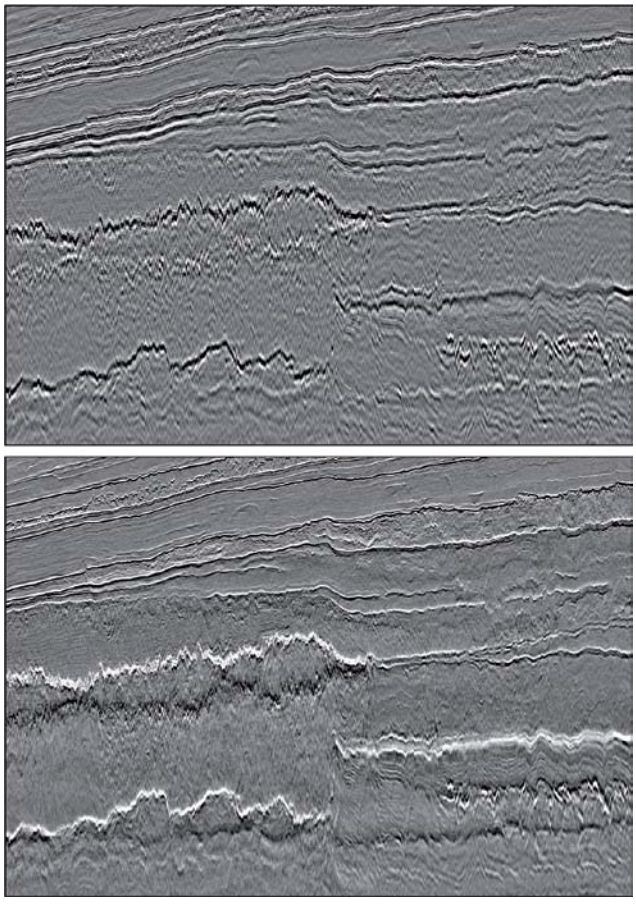

Figure 12 *Zoom in to the shallow 'blue box' area of Figure 11.*

Returning to the photographic example of Figure 1, Figure 9 repeats the top (two ghosts) and bottom (no ghosts) photos in that sequence. The effect in these photos is analogous to the effect in the seismic data, which is shown in the central part of Figure 9. The left hand panel is hydrophone-only data acquired with a streamer depth of 15 m and a conventional source towed at 7 m, whereas the right hand panel was acquired using the dual sensor streamer and time and depth blended source. The source contained two sub-sources towed at 5 m and 9 m. These plots show the effect of removing the various responses imposed by the acquisition system and earth filtering effects. In both the photos and the seismic data the left hand images are significantly de-focused, whereas the right hand images are clear and focused and show the detailed structure. The bottom two plots in Figure 9 show the spectra of the seismic data above. The left hand spectrum clearly shows the two sets of notches caused by the source and receiver ghosts and a decaying spectrum caused by the earth filtering effect. On the other hand, the right hand plot shows a flat spectrum with all these effects removed. The frequency range in these spectra is from 0 to 250 Hz, showing that there is good S/N in the data up to ~200 Hz.

The data presented so far in this section have mostly concentrated on the amplitude spectrum of the seismic data. The change in this spectrum as shown in Figure 9 is part of the reason that the data quality improves so much. However, it is important to realize that the phase change that occurs when removing the various terms in the seismic wavelet is also a key factor in the improved data quality. Figure 8 shows the seismic wavelet in raw conventional data on the left. At this stage it contains both source and receiver ghosts and the source response. Removal of these terms produces the wavelet on the right. Not only is this final wavelet zero-phase, but the ghost effects and the oscillatory bubble pulse have all been transformed into a very narrow central peak. This transformation has a very significant effect in improving the resolution of the resultant seismic data.

Data examples

Some additional data examples are shown in this section, to demonstrate the effect of removing all the acquisition-related effects, compared to conventional seismic data. These data were acquired in the Møre margin area of the Norwegian

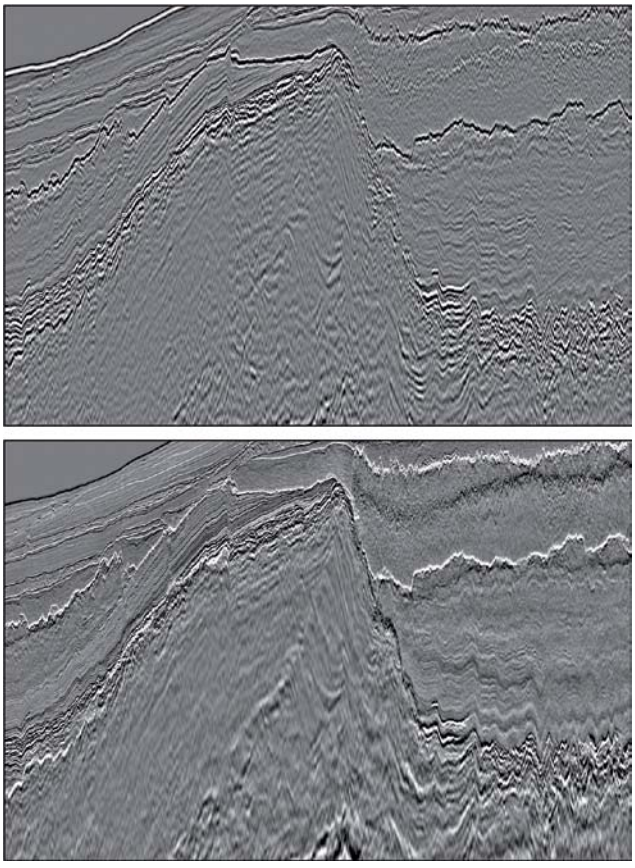

Figure 13 *Zoom in to the deeper 'blue box' area of Figure 11.*

Sea, which is a notoriously difficult imaging area. The section at the top of Figure 11 was shot in 2010 using a conventional airgun array at 9 m and a dual sensor streamer at 25 m. However, in the data shown, the total pressure field has been reconstructed at a depth of 12 m from the dual sensor data, to simulate conventional streamer data. The bottom section was shot in 2011 using a dual sensor streamer at 25 m and a time and depth blended source with two sub-sources at 10 m and 14 m. It has had all the acquisition-related effects removed, as described previously in the text.

Figures 12 and 13 show the 'blue box' regions of Figure 11 at higher resolution. The data from the new system is dramatically improved compared to conventional data and has a three-dimensional photographic quality. These latter data are very close indeed to representing the response of the earth.

Conclusions

A marine seismic acquisition system consisting of dual sensor streamers and a time and depth distributed source has been presented. This system provides an acquisition-based solution for producing ghost-free seismic data. After removing both ghosts and correcting for the source signature, the seismic data reveals the earth response. The final result is only limited by the response of the receiver system, so the resultant seismic data is broadband and focused.

Acknowledgements

We would like to thank Peter Aaron for doing such an excellent job in developing the processing techniques. We would also like to thank PGS management, operations, and data processing for their support, encouragement, and efforts throughout this work.

References

Carlson, D., Long, A., Söllner, W., Tabti, H., Tenghamn, R. and Lunde, N. [2007] Increased resolution and penetration from a towed dual-sensor streamer. *First Break*, **25**(12), 71–77.

Hegna, S., and Parkes, G. 2011, The low frequency output of marine air-gun arrays. *81st SEG Annual Meeting*. Expanded Abstracts, **30**, 77–81.

Long, A., Mellors, D., Allen, T. and McIntyre, A. [2008] A calibrated dual-sensor streamer investigation of deep target signal resolution and penetration on the NW Shelf of Australia. *78th SEG Annual Meeting*. Expanded Abstracts, **27**, 428–432.

Posthumus, B. [1993] Deghosting of twin streamer configuration. *Geophysical Prospecting*, **41**, 267–286.

Van Borselen, R., Hegge, R., Martin, T., Barnes, S. and Aaron, P. [2011] Enhanced demultiple by 3D SRME using dual-sensor measurements. The Leading Edge, 30(8), 920–926.